EDGE ARTICLE

Check for updates

Highly stable color-tunable organic long-persistent luminescence from a single-component exciplex copolymer for *in vitro* antibacterial†

Hui Li,*[a] Xiaoye Li,[b] Haoran Su,[a] Shuman Zhang,[a] Cheng Tan,[a] Cheng Chen,[a] Xin Zhang,[a] Jiani Huang,[a] Jie Gu,[a] Huanhuan Li,[a] Gaozhan Xie,[a] Heng Dong, [ID] *[b] Runfeng Chen [ID] [a] and Ye Tao [ID] *[ac]

Developing exciplex-based organic long-persistent luminescence (OLPL) materials with high stability is very important but remains a formidable challenge in a single-component system. Here, we report a facile strategy to achieve highly stable OLPL in an amorphous exciplex copolymer system *via* through-space charge transfer (TSCT). The copolymer composed of electron donor and acceptor units can not only exhibit effective TSCT for intra/intermolecular exciplex emission but also construct a rigid environment to isolate oxygen and suppress non-radiative decay, thereby enabling stable exciplex-based OLPL emission with color-tunable feature for more than 100 h under ambient conditions. These single-component OLPL copolymers demonstrate robust antibacterial activity against *Escherichia coli* under visible light irradiation. These results provide a solid example to exploit highly stable exciplex-based OLPL in polymers, shedding light on how the TSCT mechanism may potentially contribute to OLPL in a single-component molecular system and broadening the scope of OLPL applications.

Introduction

Organic long-persistent luminescence (OLPL) has drawn a lot of attention owing to its unique optical phenomenon and important applications in many fields.[1–12] A set of strategies including H-aggregation,[13,14] host–guest doping,[15,16] self-assembly,[17,18] exciplex formation[19–22] and many other methods[10] to realize OLPL have been proposed. Among them, the exciplex strategy, which utilizes the synergistic effect of long-range charge transfer and diffusion between selected donor (D) and acceptor (A) moieties to form stable radical anions and cations as well as gradual electron–hole recombination among radical anions and cations, has been proved to be one of the most successful strategies.[23–25] Over the past few years, binary D–A doping[26] and trap-assisted ternary D–A doping[20] as well as single- and multiple-component ionic crystal systems[27–29] have been reported to develop highly efficient exciplex-based OLPL materials. Despite these significant developments, most exciplex-based OLPL materials rely on multi-component charge transportation/recombination under inert environments, wherein the phase separation from a homogeneous mixture in multi-component subjects and strict operating conditions are inevitable, imposing great constraints for practical applications over long timescales.

Notably, besides a multivariate physical blending system, single-component charge-transfer emission can also be achieved by through-space charge transfer (TSCT) in a copolymer system composed of a non-conjugated polymeric backbone as well as pendant D and A units to develop efficient thermally activated delayed fluorescence (TADF) emission.[30–33] This TSCT copolymer can support efficient charge transfer to regulate singlet-triplet energy splitting and to modulate the carrier separation/recombination between the physically separated D and A units by controlling the D/A feed ratios; also, the chemically connected copolymer not only can effectively suppress phase separation for long-time operation but also may potentially facilitate the formation of an interpenetrating rigid polymeric environment for inhibition of non-radiative decay. For instance, efficient and full-color TSCT emissions can be realized between physically separated but spatially proximate D and A groups connected by non-conjugated polyethylene and/or polynorbornene backbones.[34–36] Inspired by the ingenious strategy in realizing single-component TSCT emission and physically blended exciplex-based OLPL emission, we deduce that the realization of OLPL emission in a single-component copolymer under ambient conditions is reasonable. Theoretically, by carefully implanting pendant D and A groups in a copolymer,

[a]*State Key Laboratory of Organic Electronics and Information Displays, Institute of Advanced Materials (IAM), Nanjing University of Posts & Telecommunications, 9 Wenyuan Road, Nanjing 210023, China. E-mail: iamhli@njupt.edu.cn; iamytao@njupt.edu.cn*

[b]*Nanjing Stomatological Hospital, Affiliated Hospital of Medical School, Research Institute of Stomatology, Nanjing University, 30 Zhongyang Road, Nanjing, Jiangsu 210008, China. E-mail: dongheng90@smail.nju.edu.cn*

[c]*Songshan Lake Materials Laboratory, Dongguan, Guangdong 523808, China*

† Electronic supplementary information (ESI) available. See DOI: https://doi.org/10.1039/d4sc02839b
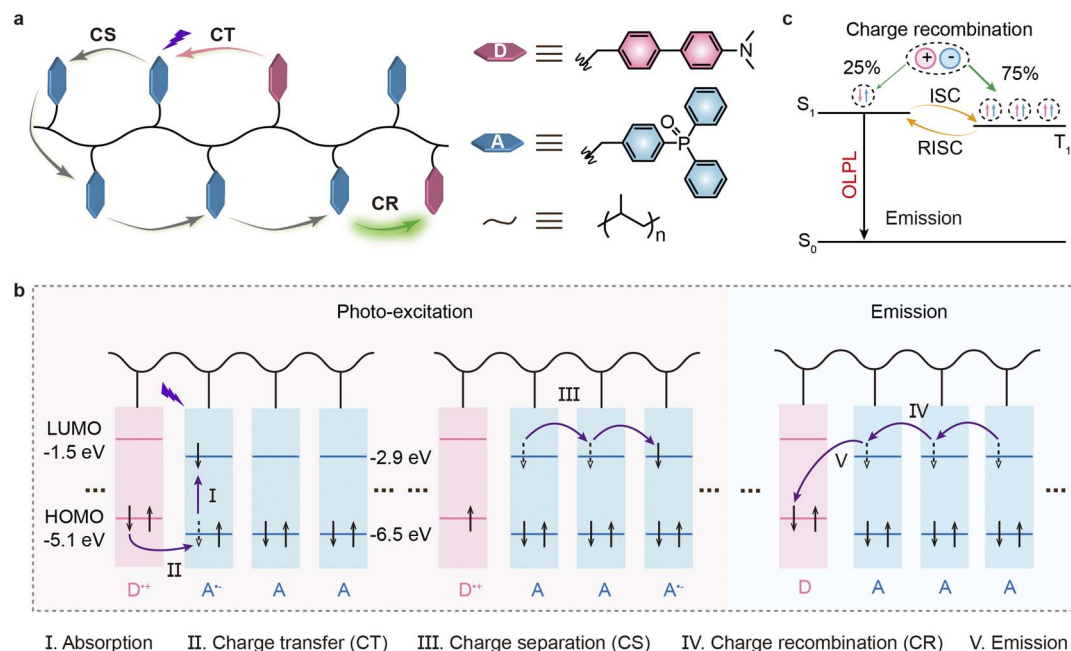
Fig. 1 Schematic representation and mechanism for achieving single-component OLPL polymers. (a) An illustration of a single-component OLPL polymer and chemical structures of the copolymer as well as a plausible OLPL process under UV light. (b) OLPL mechanism of copolymer materials. (c) Exciton generation and utilization in OLPL materials after charge recombination.

the efficient TSCT effect to facilitate the charge transfer process for achieving charge separation between D and A moieties could be anticipated, thus allowing the formation of stable radical anions and cations; thereafter, electrons stabilized by the radical anions can hop among the acceptors for the formation of a stable charge separation state. Eventually, the gradual recombination of electrons and holes originating from radical anions and cations could enable OLPL emission.

To verify our deduction, we design and synthesize a class of exciplex-based OLPL materials through efficient TSCT in a single-component copolymer system by bonding the strong electron-donating molecule N,N-dimethyl-4'-vinyl-[1,1'-biphenyl]-4-amine (**DMB**) and the strong electron-accepting molecule diphenyl(4-vinylphenyl)phosphine oxide (**DPPO**) in a non-conjugated polyethylene backbone (Fig. 1a).[37,38] In this design, **DMB** forms a quite stable cation and the phosphine-oxide-based **DPPO** can not only allow effective charge separation to achieve a stable anion upon interacting with **DMB** but also afford a rigid environment to suppress non-radiative decay for the realization of OLPL emission. Notionally, an exciplex can boost an effective charge transfer (CT, II) process between the highest occupied molecular orbitals (HOMOs) of **DMB** and **DPPO** (Fig. 1b), thus facilitating the construction of stable radical anions and cations; then, electrons can hop from stable **DPPO** radical anions to **DPPO** to form charge-separated states (CS, III). Finally, the gradual charge recombination (CR, IV) of **DPPO** radical anions and **DMB** radical cations produces OLPL emission (V). OLPL lasts for a long time after photoexcitation ceases. And, because of the small splitting energy between singlet and triplet states (ΔE_{ST}) of the TSCT polymer, efficient intersystem crossing (ISC) and reverse ISC (RISC) to boost TADF emission can be achieved (Fig. 1c) for utilization of triplet excitons. Indeed, stable OLPL from a single-component

amorphous copolymer was readily achieved and this OLPL emission can remain for more than 100 h under ambient conditions without any encapsulation. More significantly, owing to their highly efficient generation of triplet excitons, OLPL polymers can effectively eliminate at least 78.24% of *Escherichia coli* (*E. coli*) when exposed to visible light irradiation via photodynamic therapy. This demonstrates promising antibacterial results for *in vitro* applications. Our work in purposefully designing and developing single-component exciplex-based OLPL materials through an ingenious TSCT tactic may not only open up a new way for the development of highly stable OLPL but also further propel the application of exciplex-based OLPL in the field of biology.

Results and discussion

Molecular design and characterization

Three copolymers, **PDD-99**, **PDD-199** and **PDD-299**, were synthesized by radical polymerization of **DMB** and **DPPO** monomers with different molar feed ratios of 1 : 99, 1 : 199 and 1 : 299, respectively. In addition, we prepared the homopolymer **P-DPPO** through the radical polymerization of **DPPO** for further study of the stable exciplex-based OLPL emission mechanism. The chemical structures of these polymers were characterized by nuclear magnetic resonance spectra, gel permeation chromatography and Fourier transform infrared spectra (Scheme S1, Fig. S1–S7 and Table S1†). Powder X-ray diffraction analysis, thermal property analyses and electrochemical properties are presented in the ESI (Fig. S8–S10 and Table S2†). **PDD-99, PDD-199** and **PDD-299** can form an amorphous state in the solid form (Fig. S8†) and display good thermal stability (Fig. S9†). The HOMO energy levels of **DPPO** and **DMB** were estimated from the onset of the oxidative wave of cyclic voltammetry (CV)

experiments (Fig. S10 and Table S2†). And with the aid of optical bandgaps (E_g) determined from the absorption spectra, the lowest unoccupied molecular orbital (LUMO) levels of **DMB** and **DPPO** were deduced to be −1.52 and −2.91 eV, respectively. The matched energy levels of the HOMO and LUMO indicate that efficient exciplex emission can be achieved between **DMB** and **DPPO**. To gain insight into the electron features of the copolymers, theoretical calculations of HOMO and LUMO electron density and their orbital energy levels were performed. The modeled polymers composed of **DMB** and **DPPO** units in molar ratios of 1 : 2, 1 : 5 and 1 : 10 were constructed. As expected, the frontier molecular orbital distributions of HOMO and LUMO localize on the **DMB** and **DPPO** (Fig. S11†), respectively, which indicate the TSCT characteristics of the copolymers. And the separated frontier molecular orbitals enable a small ΔE_{ST} that facilitates efficient ISC and RISC processes through regulating the molar feed ratios between **DMB** and **DPPO** units (Fig. S12†).

Photophysical properties

PDD-99, **PDD-199** and **PDD-299** powders show broad featureless steady-state photoluminescence (SSPL) spectra with main emission peaks at ∼486 nm, which is substantially redshifted compared to the SSPL emission of **DMB** and **DPPO** monomers (Fig. 2a, S13 and S14†). Moreover, the broad SSPL band of **PDD-299** shows strong dependence on solvent polarities (Fig. S15†). These results indicate a distinct CT transition between the **DMB** and **DPPO** units in **PDD-299**, suggesting the formation of an exciplex in these single-component copolymers through TSCT.[39,40] Strikingly, after turning off the excitation source, **PDD-99**, **PDD-199** and **PDD-299** powders exhibit a notable emission with broad OLPL bands (delayed time: 10 ms) at about 486 nm with lifetimes of about 500 ms (Fig. 2a, b, S16, S17 and Table S3†); and, with short delayed time (2 ms), simultaneous emissions involving OLPL (486 nm) and room temperature phosphorescence (530 nm) are observed (Fig. 2a), indicating the presence of multiple luminescent centers (Fig. S18†). The behavior of the lifetime decay profiles of the OLPL band in **PDD-299** powder exhibits inverse-power functions of time t^{-m} (m = 0.9), which indicates the presence of CS intermediate states (Fig. 2b) as testified by electron paramagnetic resonance (EPR) measurements showing an enhanced signal after UV excitation (Fig. S19†). These results demonstrate that OLPL from a single-component exciplex copolymer was achieved, though there is still a huge gap in the OLPL duration compared to the reported multi-component systems, possibly due to the fast intra-/intermolecular CR between the **DMB** and **DPPO** units in the copolymer. The decay profiles of single-component OLPL copolymers closely depend on the molar feed ratios of the **DMB** and **DPPO** units and the intensity of excitation light, which are similar to multi-component OLPL systems.[41] When the molar feed ratio between **DMB** and **DPPO** units changes from 1 : 99 (**PDD-99**) to 1 : 199 (**PDD-199**) to 1 : 299 (**PDD-299**), the duration of OLPL is significantly improved (Fig. 2b, S16 and S17†). The increased OLPL features may be attributed to the enlarged distance between **DMB** and **DPPO** units for reducing the recombination probability of radical cations and anions at higher molar concentrations of **DPPO** units. The OLPL can be facilely excited by low excitation power and the OLPL properties of **PDD-99**, **PDD-199** and **PDD-299** gradually increase when the excitation power density increases from 3.3 to 13.9 mW cm^{-2} (Fig. 2b, S16 and S17†). These results clearly indicate the gradual accumulation of charge carriers in the developed copolymers. To explore the influence of temperature on the
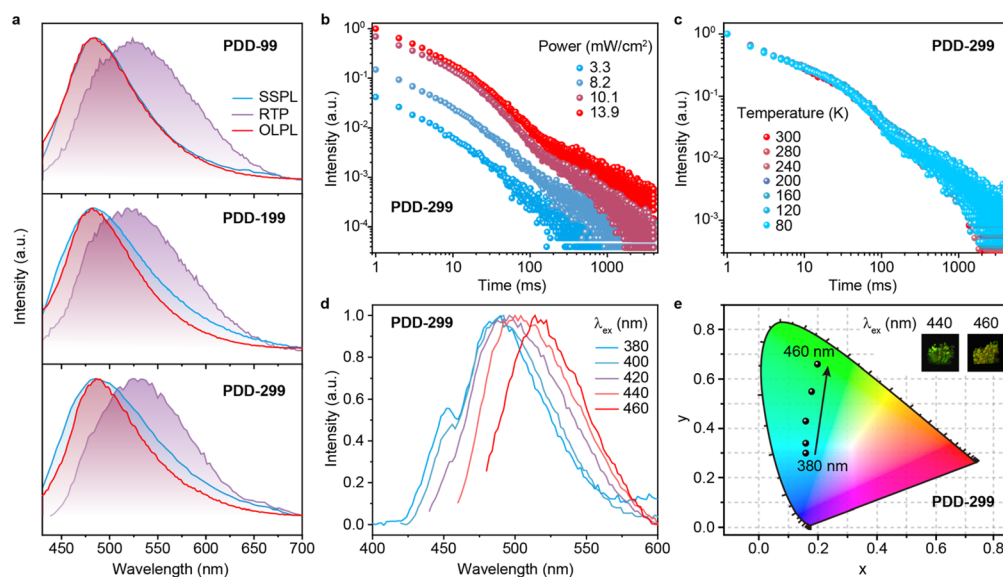

Fig. 2 Photophysical properties of OLPL polymer powders. (a) Steady-state PL, room temperature phosphorescence (delayed time: 2 ms) and OLPL (delayed time: 10 ms) spectra of **PDD-99**, **PDD-199** and **PDD-299** (λ_{ex} = 410 nm) under ambient conditions. (b) Excitation intensity-dependent OLPL decay profiles (λ_{em} = 486 nm) of **PDD-299** under ambient conditions. (c) Temperature-dependent OLPL decay profiles (λ_{em} = 486 nm) of **PDD-299** ranging from 300 to 80 K. (d) OLPL spectra (delayed time: 10 ms) and (e) corresponding CIE coordinates of **PDD-299** under different excitation wavelengths under ambient conditions.
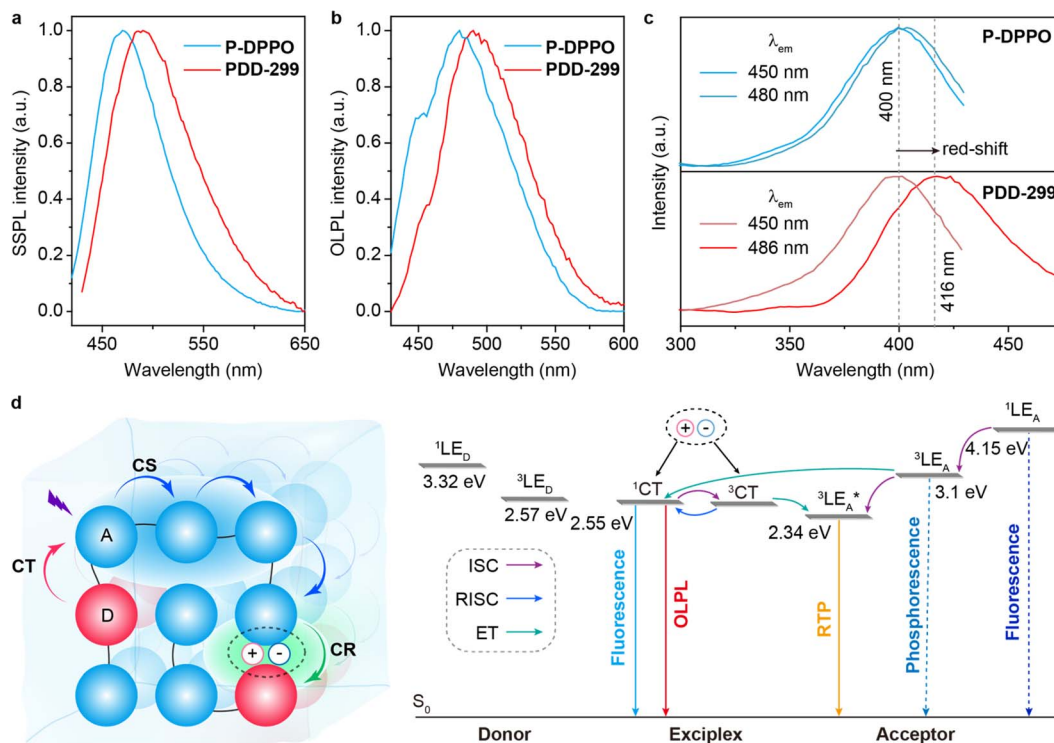
Fig. 3 Proposed mechanism of OLPL materials under ambient conditions. SSPL (a) and OLPL (b, delayed time: 10 ms) spectra of **P-DPPO** and **PDD-299** powders. (c) Excitation spectra for **P-DPPO** and **PDD-299** powders through monitoring various OLPL emission peaks. (d) Scheme for the formation of radical pair through CT, CS and CR processes (left) and plausible energy transfer processes to achieve exciplex–based OLPL emission from a single–component copolymer system.

exciplex-based OLPL, OLPL decay measurements of **PDD-299** at different temperatures were carried out (Fig. 2c). The stable decay profiles varied from 80 to 300 K indicate that non-radiative transitions by molecular vibrations have been nearly suppressed in **PDD-299** powder. The decay profiles of **PDD-99** and **PDD-199** powders exhibit the same trend as those of **PDD-299** (Fig. S20†), showing stable decay profiles at temperatures below 300 K. However, at higher temperatures, the duration for **PDD-299** is significantly reduced (Fig. S21†). The suppressed non-radiative deactivation at room temperature may be due to the fact that the main unit of **DPPO** provides a dense and rigid network environment within the copolymer.

Surprisingly, color-tunable OLPL is observed in the single-component copolymers under different excitation (Fig. 2d, S22 and S23†). With a change of excitation wavelength from 380 nm to 460 nm, the OLPL spectra of **PDD-299** exhibit a significant redshift from blue-green to yellowish-green with the main peaks from 480 to 520 nm (Fig. 2d), respectively. **PDD-99** and **PDD-199** also show obvious color-tunable OLPL emissions with varied emission peaks ranging from 480 to 520 nm when the excitation wavelength is changed from 380 nm to 460 nm (Fig. S22 and S23†) and the corresponding Commission International de l'Eclairage (CIE) coordinates present obvious excitation-dependent properties. As shown in Fig. S24,† the lifetimes of **PDD-99**, **PDD-199** and **PDD-299** initially increase when the excitation wavelength increases from 360 to 420 nm, and then the lifetimes gradually decrease when the excitation wavelength

increases from 420 to 460 nm. To investigate the origin of the color-tunable properties of the copolymers, we measured the OLPL spectra and decay profiles of homopolymer **P-DPPO** (Fig. S25 and S26†). The OLPL spectra of **P-DPPO** exhibit obvious excitation-dependent properties (Fig. S25†), showing varied main emission peaks ranging from 450 to 480 nm when the excitation wavelength is changed from 350 to 430 nm. By comparing the excitation-dependent OLPL spectra between the **PDD** copolymers and **P-DPPO** (Fig. S22, S23, and S25†), the main emission peak ranging from 450 to 480 nm of the **PDD** copolymers should mainly derive from **P-DPPO** due to the major components of **DPPO** units in the **PDD** copolymers; besides, the emission peaks ranging from 480 to 520 nm of the **PDD** copolymers should principally be caused by exciplex emission. Therefore, the color-tunable OLPL emission in the **PDD** copolymers may arise from different luminescent centers including homopolymer **P-DPPO** and exciplex emission upon being excited at different wavelengths.

Mechanism of OLPL polymers

To further verify the involvement of dual luminescent centers in exciplex-based OLPL, additional photophysical property investigations based on **PDD-299** and **P-DPPO** were carried out. Compared to **P-DPPO**, **PDD-299** exhibits broader and red-shifted SSPL and OLPL spectra (Fig. 3a and b), suggesting again the existence of an exciplex as verified by the red-shifted excitation spectra (Fig. 3c and S27†). Moreover, **PDD-299**

exhibits a main excitation peak at ~416 nm and a shoulder peak at ~400 nm, similar to **P-DPPO** (Fig. 3c). Interestingly, with decreasing temperature, a red-shifted emission peak from 520 to 550 nm is observed and becomes the dominant emission in the OLPL spectra of **PDD-299** powder, which is also identical to that of the **P-DPPO** powder (Fig. S28†), indicating that the emission from homopolymer **P-DPPO** should be involved in the emission of PDD polymers. To figure out the origin of the emission bands at 530 nm, the concentration-dependent OLPL emission based on **P-DPPO** was studied. Red-shifted emission bands from 500 to 520 nm are observed with increasing concentration of **P-DPPO** from 1.5 to 20 mg mL^{-1} (Fig. S29†) in solution, thus suggesting that the emission peaks from 520 to 550 nm may derive from the radiative decay from the **DPPO** aggregates due to the shortened distance between **DPPO** units at low temperatures.[42] These observations provide further evidence that the OLPL emission in the PDD copolymers arises from the two emissive species including homopolymer **P-DPPO** and exciplex emission.

Based on the comprehensive experimental findings, we can propose a plausible mechanism for achieving OLPL in a single-component copolymer system through TSCT under ambient conditions, as illustrated in Fig. 3d. Under photoexcitation, the copolymer system can effectively achieve CT, CS and CR processes between donor and acceptor units to enable exciplex-based OLPL emission. The effective separation of the HOMO on donor and LUMO on acceptor in the exciplex results in a minimal energy gap between the lowest excited singlet (^{1}CT) and triplet (^{3}CT) states of the exciplex.[43–45] After the CR process, ^{1}CT and ^{3}CT excitons are generated. Due to the small energy gap between ^{1}CT and the lowest triplet energy of acceptor (^{3}LE$_A$), the processes of ISC and RISC could occur, which is like the process in TADF materials, thus affording OLPL emission from ^{1}CT of the exciplex. Furthermore, as the main component in the copolymer, unit A can also realize OLPL emission, enabling the co-occurrence of emission from exciplex and homopolymer for color-tunable OLPL under different excitations. Notably, due to the relatively large energy gap between ^{1}CT and ^{3}LE$_A^*$ of aggregates, the TADF activity between ^{1}CT and ^{3}LE$_A^*$ is significantly suppressed, thus leading to much enhanced phosphorescence from aggregates under cryogenic conditions.

Stability performance of OLPL polymers

To verify the much-enhanced stability of exciplex-based OLPL from the single-component copolymer system, a binary
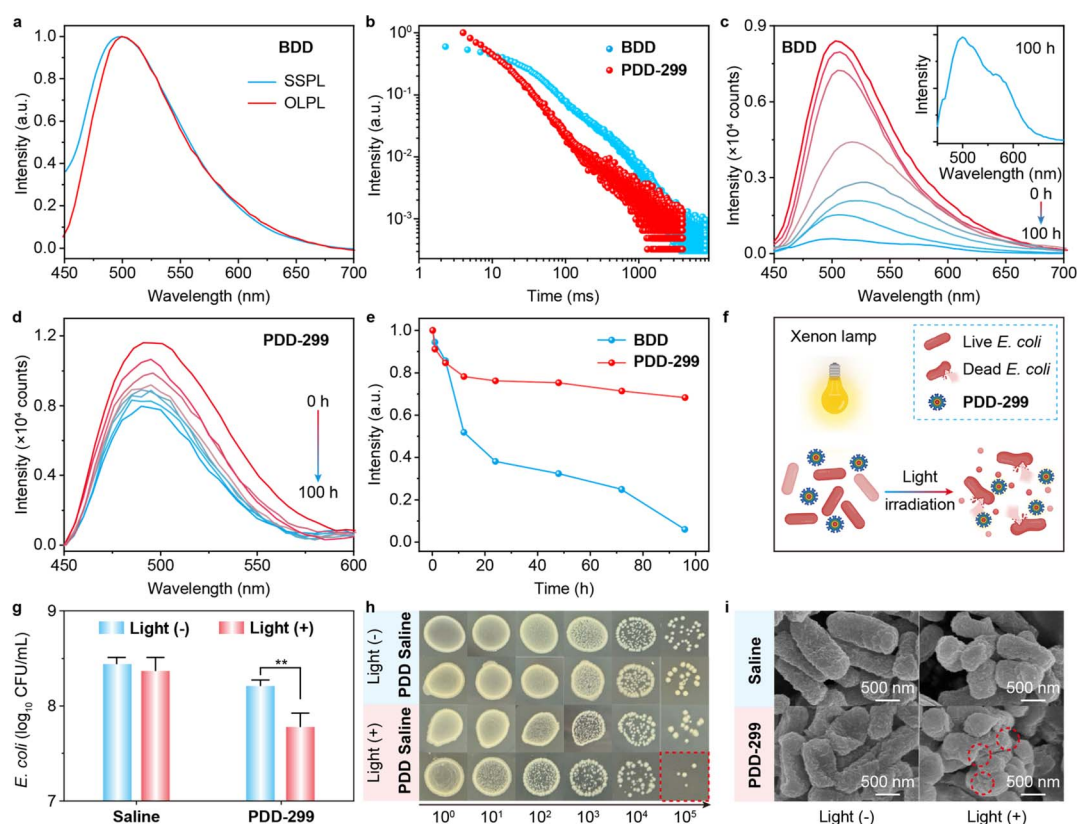

Fig. 4 Stability properties and *in vitro* antibacterial activity of OLPL polymers. (a) SSPL and OLPL (delayed time: 10 ms) spectra of **BDD** under ambient conditions. (b) Decay profiles of OLPL emission of **BDD** (λ_{em} = 500 nm) and **PDD-299** (λ_{em} = 486 nm) under ambient conditions. (c–e) OLPL spectra ((c) and (d); delayed time: 10 ms) and corresponding intensity profiles (e) of **BDD** (c) and **PDD-299** (d) at different kept times under ambient conditions. Inset shows the OLPL (delayed time: 10 ms) spectrum of **BDD** after being placed in the atmosphere for 100 hours. Note that the excitation wavelength is fixed at 410 nm. (f) Schematic illustration of the inactivation of *E. coli* killed by **PDD-299** under light irradiation. CFU number (g) and original images (h) of *E. coli* after different treatments (n = 3; mean ± SD). (i) Scanning electron microscope (SEM) images of *E. coli* after different treatments; red circles indicate bacterial structural damage.

exciplex **BDD** was prepared by physically blending **DMB** and **DPPO** at a molar ratio of 1 : 299. As shown in Fig. 4a, the **BDD** powder shows almost uniform SSPL and OLPL spectra. Compared to SSPL spectra of **DMB** and **DPPO**, the red-shifted and broad featureless SSPL spectra of **BDD** confirm the formation of the exciplex. The decay profiles exhibit obvious power-law emission behavior, which demonstrates that the OLPL emission of **BDD** also originates from intermediate CS states (Fig. 4b). Although **BDD** exhibits slightly longer decay times than **PDD-299**, the stability of **BDD** is significantly lower than that of **PDD-299** under ambient conditions. Compared to the pristine state (Fig. 4c–e), after being kept for 100 hours under ambient conditions, the OLPL intensity of **BDD** is largely decreased. In contrast, **PDD-299** powder exhibits excellent stability (Fig. 4d), showing obvious OLPL emission with a retained OLPL intensity of 70% (Fig. 4e) after being placed for 100 hours under ambient conditions. The poor long-term stability of **BDD** may be caused by phase separation of the multi-component host–guest system, thus leading to the aggregation of **DPPO** units. **PDD-299** powder presents a much stabler exciplex-based OLPL in a variety of atmospheres than multi-component OLPL materials that need inert environments (Fig. S30†), showing slightly enhanced OLPL intensity in argon and decreased OLPL intensity in oxygen compared to that in air.

In vitro antibacterial activity of OLPL polymers

In light of the effective population of triplet excitons through gradual recombination of radical anions and radical cations, we investigated the potential application of **PDD-299** as an *in vitro* antibacterial (Fig. 4f) through photodynamic therapy for generation of singlet oxygen (Fig. S31†). The generated singlet oxygen can disrupt the antioxidant defense mechanisms of bacterial cells, ultimately leading to the bacterial damage and death. *E. coli*, a typical Gram-negative bacterium, which can pose potential harm to human health, was selected. Here, using visible light as the excitation source and physiological saline as a standard reference, we investigated the bactericidal capability of **PDD-299** through plate colony counting. The 78.24% inactivation efficiency of *E. coli* induced by **PDD-299** after continuous irradiation under visible light for 4 h is significantly higher compared to the inactivation efficiency of saline and the control group without light irradiation (Fig. 4g and h); these results are comparable to those for recently reported *in vitro* antibacterial materials (Table S4†).[46–50] Compared to *E. coli* treated with saline, which remained intact or was slightly wrinkled after light irradiation, the membrane of *E. coli* cells treated with **PDD-299** showed significant structural damage after light irradiation (Fig. 4i), further indicating the exceptional antibacterial capability of **PDD-299** under visible light irradiation.

Conclusions

In summary, we have succeeded in proposing an ingenious approach to achieve color-tunable exciplex-based OLPL with high stability in an amorphous single-component copolymer system. The tactic involves the effective charge transfer between **DMB** donor and **DPPO** acceptor through TSCT to enable stable radical anions and cations for affording intra/intermolecular exciplex emission. The single-component copolymers yield quite stable exciplex-based OLPL emission for 100 h under various atmospheres due to the rigid polymer for isolating oxygen and suppressing non-radiative decay. In addition, benefiting from the dual luminescent centers of localized emissions from **DPPO** homopolymer and charge transfer exciplex, color-tunable single-component OLPL polymers are also realized under different excitation wavelengths. Moreover, the single-component OLPL copolymer system disrupts the cell membrane of *E. coli* upon light irradiation, resulting in *E. coli* inactivation and showcasing an outstanding antibacterial performance. This study provides a simple molecular design strategy for the development of amorphous single-component exciplex-based OLPL materials, offering an important insight into the construction of highly stable OLPL materials and expansion of OLPL applications.

Data availability

All the necessary data to support the findings of this study can be found within the main text and ESI.†

Author contributions

H. L., H. D. and Y. T. conceived and designed the experiments. H. L., H. S. and S. Z. were primarily responsible for the experiments. H. L., C. T., C. C., H. L. and J. G. measured and analyzed the photophysical properties. X. Z., J. H. and G. X. performed the computational calculations. X. L. and H. D. performed the application of *vitro* antibacterial. H. L., H. D., R. C. and Y. T. wrote the manuscript and all authors contributed to the data analysis.

Conflicts of interest

There are no conflicts to declare.

Acknowledgements

References

1 R. Kabe and C. Adachi, *Nature*, 2017, **550**, 384–387.

2 W. Zhao, Z. He and B. Z. Tang, *Nat. Rev. Mater.*, 2020, **5**, 869–885.

3 E. Hamzehpoor, C. Ruchlin, Y. Tao, C. Liu, H. M. Titi and D. F. Perepichka, *Nat. Chem.*, 2022, **15**, 83–90.

4 H. Li, X. Xue, Y. Cao, H. Cheng, A. Luo, N. Guo, H. Li, G. Xie, Y. Tao, R. Chen and W. Huang, *J. Am. Chem. Soc.*, 2023, **145**, 7343–7351.

5 Y. Liang, C. Xu, H. Zhang, S. Wu, J. A. Li, Y. Yang, Z. Mao, S. Luo, C. Liu, G. Shi, F. Sun, Z. Chi and B. Xu, *Angew. Chem., Int. Ed.*, 2023, **62**, e202217616.

6 Y. Liang, M. Liu, T. Wang, J. Mao, L. Wang, D. Liu, T. Wang and W. Hu, *Adv. Mater.*, 2023, **35**, 2304820.

7 Y. Zhao, B. Ding, Z. Huang and X. Ma, *Chem. Sci.*, 2022, **13**, 8412–8416.

8 W. Ye, H. Ma, H. Shi, H. Wang, A. Lv, L. Bian, M. Zhang, C. Ma, K. Ling, M. Gu, Y. Mao, X. Yao, C. Gao, K. Shen, W. Jia, J. Zhi, S. Cai, Z. Song, J. Li, Y. Zhang, S. Lu, K. Liu, C. Dong, Q. Wang, Y. Zhou, W. Yao, Y. Zhang, H. Zhang, Z. Zhang, X. Hang, Z. An, X. Liu and W. Huang, *Nat. Mater.*, 2021, **20**, 1539–1544.

9 Y. Zhang, L. Gao, X. Zheng, Z. Wang, C. Yang, H. Tang, L. Qu, Y. Li and Y. Zhao, *Nat. Commun.*, 2021, **12**, 2297.

10 Y. Miao, F. Lin, D. Guo, J. Chen, K. Zhang, T. Wu, H. Huang, Z. Chi and Z. Yang, *Sci. Adv.*, 2024, **10**, eadk3354.

11 C. Ji, L. Lai, P. Li, Z. Wu, W. Cheng and M. Yin, *Aggregate*, 2021, **2**, e39.

12 B. Fang, L. Lai, M. Fan and M. Yin, *J. Mater. Chem. C*, 2021, **9**, 11172–11179.

13 Y. Tao, C. Liu, Y. Xiang, Z. Wang, X. Xue, P. Li, H. Li, G. Xie, W. Huang and R. Chen, *J. Am. Chem. Soc.*, 2022, **144**, 6946–6953.

14 H. Li, H. Li, J. Gu, F. He, H. Peng, Y. Tao, D. Tian, Q. Yang, P. Li, C. Zheng, W. Huang and R. Chen, *Chem. Sci.*, 2021, **12**, 3580–3586.

15 Y. Wang, H. Gao, J. Yang, M. Fang, D. Ding, B. Z. Tang and Z. Li, *Adv. Mater.*, 2021, **33**, 2007811.

16 Y. Xia, C. Zhu, F. Cao, Y. Shen, M. Ouyang and Y. Zhang, *Angew. Chem., Int. Ed.*, 2023, **62**, e202217547.

17 F. Nie, K. Z. Wang and D. Yan, *Nat. Commun.*, 2023, **14**, 1654.

18 G. Yin, W. Lu, J. Huang, R. Li, D. Liu, L. Li, R. Zhou, G. Huo and T. Chen, *Aggregate*, 2023, **4**, e344.

19 K. Jiang, Y. Wang, C. Lin, L. Zheng, J. Du, Y. Zhuang, R. Xie, Z. Li and H. Lin, *Light Sci. Appl.*, 2022, **11**, 80.

20 K. Jinnai, R. Kabe, Z. Lin and C. Adachi, *Nat. Mater.*, 2022, **21**, 338–344.

21 Z. Lin, R. Kabe, K. Wang and C. Adachi, *Nat. Commun.*, 2020, **11**, 191.

22 Y. Zhou, P. Zhang, Z. Liu, W. Yan, H. Gao, G. Liang and W. Qin, *Adv. Mater.*, 2024, 2312439.

23 A. Cheng, H. Su, X. Gu, W. Zhang, B. Zhang, M. Zhou, J. Jiang, X. Zhang and G. Zhang, *Angew. Chem., Int. Ed.*, 2023, **62**, e202312627.

24 Y. Zhao, B. Ding, Z. Huang and X. Ma, *Chem. Sci.*, 2022, **13**, 8412–8416.

25 W. Li, Z. Li, C. Si, M. Y. Wong, K. Jinnai, A. K. Gupta, R. Kabe, C. Adachi, W. Huang, E. Zysman-Colman and I. D. W. Samuel, *Adv. Mater.*, 2020, **32**, 2003911.

26 W. Qiu, X. Cai, M. Li, Z. Chen, L. Wang, W. Xie, K. Liu, M. Liu and S. Su, *J. Phys. Chem. Lett.*, 2021, **12**, 4600–4608.

27 P. Alam, T. S. Cheung, N. L. C. Leung, J. Zhang, J. Guo, L. Du, R. T. K. Kwok, J. W. Y. Lam, Z. Zeng, D. L. Phillips, H. H. Y. Sung, I. D. Williams and B. Z. Tang, *J. Am. Chem. Soc.*, 2022, **144**, 3050–3062.

28 S. Garain, S. M. Wagalgave, A. A. Kongasseri, B. C. Garain, S. N. Ansari, G. Sardar, D. Kabra, S. K. Pati and S. J. George, *J. Am. Chem. Soc.*, 2022, **144**, 10854–10861.

29 P. Alam, N. L. C. Leung, J. Liu, T. S. Cheung, X. Zhang, Z. He, R. T. K. Kwok, J. W. Y. Lam, H. H. Y. Sung, I. D. Williams, C. C. S. Chan, K. S. Wong, Q. Peng and B. Z. Tang, *Adv. Mater.*, 2020, **32**, 2001026.

30 S. Shao, J. Hu, X. Wang, L. Wang, X. Jing and F. Wang, *J. Am. Chem. Soc.*, 2017, **139**, 17739–17742.

31 J. Poisson, C. M. Tonge, N. R. Paisley, E. R. Sauvé, H. Mcmillan, S. V. Halldorson and Z. M. Hudson, *Macromolecules*, 2021, **54**, 2466–2476.

32 C. M. Tonge and Z. M. Hudson, *J. Am. Chem. Soc.*, 2019, **141**, 13970–13976.

33 Y. Xin, Y. Zhu, R. Chi, C. Duan, P. Yan, C. Han and H. Xu, *Adv. Mater.*, 2023, **35**, 2304103.

34 J. Hu, Y. Wang, Q. Li, S. Shao, L. Wang, X. Jing and F. Wang, *Chem. Sci.*, 2021, **12**, 13083–13091.

35 J. Hu, Q. Li, X. Wang, S. Shao, L. Wang, X. Jing and F. Wang, *Angew. Chem., Int. Ed.*, 2019, **58**, 8405–8409.

36 S. Ye, N. Meftahi, I. Lyskov, T. Tian, R. Whitfield, S. Kumar, A. J. Christofferson, D. A. Winkler, C. Shih, S. Russo, J. Leroux and Y. Bao, *Chem*, 2023, **9**, 924–947.

37 D. Zhong, X. Yang, X. Deng, X. Chen, Y. Sun, P. Tao, Z. Li, J. Zhang, G. Zhou and W. Wong, *Chem. Eng. J.*, 2023, **452**, 139480.

38 K. Jinnai, R. Kabe and C. Adachi, *Adv. Mater.*, 2018, **30**, 1800365.

39 S. Kumar, L. G. Franca, K. Stavrou, E. Crovini, D. B. Cordes, A. M. Z. Slawin, A. P. Monkman and E. Zysman-Colman, *J. Phys. Chem. Lett.*, 2021, **12**, 2820–2830.

40 S. Yang, Y. Zhang, F. Kong, Y. Yu, H. Li, S. Zou, A. Khan, Z. Jiang and L. Liao, *Chem. Eng. J.*, 2021, **418**, 129366.

41 S. Tan, K. Jinnai, R. Kabe and C. Adachi, *Adv. Mater.*, 2021, **33**, 2008844.

42 Y. Shen, H. Liu, J. Cao, S. Zhang, W. Li and B. Yang, *Phys. Chem. Chem. Phys.*, 2019, **21**, 14511–14515.

43 Z. Q. Feng, S. Y. Yang, F. C. Kong, Y. K. Qu, X. Y. Meng, Y. J. Yu, D. Y. Zhou, Z. Q. Jiang and L. S. Liao, *Adv. Funct. Mater.*, 2023, **33**, 2209708.

44 D. Barman, M. Annadhasan, A. P. Bidkar, P. Rajamalli, D. Barman, S. S. Ghosh, R. Chandrasekar and P. K. Iyer, *Nat. Commun.*, 2023, **14**, 6648.

45 X. Ban, T. Zhou, K. Zhang, Q. Cao, F. Ge, D. Zhang, P. Zhu, Z. Liu, Z. Li and W. Jiang, *Chem. Eng. J.*, 2022, **441**, 135898.

46 Y. Cai, W. Cheng, C. Ji, Z. Su and M. Yin, *Dyes Pigm.*, 2021, **195**, 109698.

47 X. Fu, X. Zhao, L. Chen, P. Ma, T. Liu and X. Yan, *Biomater. Sci.*, 2023, **11**, 5186–5194.

48 L. Xu, K. Zhou, H. Ma, A. Lv, D. Pei, G. Li, Y. Zhang, Z. An, A. Li and G. He, *ACS Appl. Mater. Interfaces*, 2020, **12**, 18385–18394.

49 Y. Miao, X. Zhang, J. Li, W. Yang, X. Huang and J. Lv, *RSC Adv.*, 2022, **12**, 20481–20491.

50 C. Chao, L. Kang, W. Dai, C. Zhao, J. Shi, B. Tong, Z. Cai and Y. Dong, *J. Mat. Chem. B*, 2023, **11**, 3106–3112.